# Charge Induced (1×3) Reconstruction of the Au(110) Surface: An X-Ray Scattering Study

B. M. Ocko, G. Helgesen, Bruce Schardt, and Jia Wang
*Physics Department, Brookhaven National Laboratory, Upton, New York 11973*

A. Hamelin
*Laboratoire d'Electrochimie Interfaciale du Centre National de la Recherche Scientifique, 1, Place Aristide Briand, 92195 Meudon, France*

(Received 10 January 1992; revised manuscript received 19 August 1992)

*In situ* x-ray scattering studies of the Au(110) electrode surface have been carried out in 0.1*M* NaF, NaCl, NaBr, LiCl, CsCl, and $HClO_4$ solutions under potential control. At sufficiently negative potentials, in the salt solutions the surface forms a (1×3) reconstruction rather than a (1×2) reported for the clean vacuum surface. Above a critical threshold potential, the (1×3) reconstruction vanishes and the surface forms a (1×1) structure.

PACS numbers: 68.35.Bs, 61.10.Lx, 82.45.+z

The atomic arrangement at an electrode surface plays a vital role in determining its electrochemical properties. Detailed measurements of the atomic scale structure of electrode surfaces are now possible because of recent developments in scanning tunneling microscopy (STM) [1,2], atomic force microscopy (AFM) [3], and surface x-ray scattering (SXS) [4,5]. Here we report the results of SXS measurements which demonstrate that it is possible to modify the structure of a Au(110) surface by changing the applied potential in an electrochemical cell. By charging the surface negatively the gold surface changes from a perfectly terminated (1×1) structure to a (1×3) superstructure. In vacuum, it has been reported that the (1×2) structure, observed for clean (uncharged) surfaces [6,7], transforms to a (1×3) structure after adsorption of submonolayers of K or Cs [8,9]. The ability to electrochemically modify the reconstruction from the "clean vacuum" structure was not expected from previous studies of Au(001) and Au(111) surfaces [1,5]. Our results help elucidate the emerging relationship between vacuum and electrochemical interfaces.

The clean Au(110) surface under ultrahigh-vacuum (UHV) conditions exhibits a (1×2) missing row structure [Fig. 1(a)], where every other row along the ⟨001⟩ direction is absent [6,7]. The ability to electrochemically induce a reconstructed Au(110) surface in salt solutions was suggested on the basis of the frequency dispersion in the double-layer capacitance [10]. Previous low energy electron diffraction (LEED) [11] and STM [12] studies of Au(110) electrodes suggest that the Au(110) surface forms a reconstructed phase, but these studies have not provided a complete and unambiguous interpretation. In the *ex situ* LEED study [11] the (1×2) reconstruction appears to be stable well into the positive charge regime. This finding is not supported by our results or by STM, both of which are carried out *in situ*. Both (1×2) and (1×3) domains are reported in the STM study; however, the relationship between these two coexisting local structures is never established. Furthermore an anomalously large lateral distortion in the second atomic layer [12] is reported. In order to resolve these questions, and to understand the effects of surface charge on the structure of the Au(110) electrode we have carried out a comprehensive x-ray scattering study in salt and acid solutions.

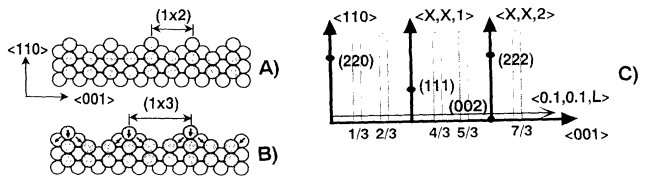


FIG. 1. Cross-sectional view of the (a) (1×2) and (b) (1×3) missing-row models of the reconstructed Au(110) surface. The surface scattering geometry is shown in (c).

*In situ* SXS measurements were made with gold disk electrodes (3 mm by 10 mm diameter) with the surface normal vector (optical axis) aligned to within 0.05° of the (110) crystallographic planes. The Au(110) crystal used for the present study forms a LEED pattern in vacuum characteristic of a well-ordered (1×2) reconstruction [13]. After a final sputtering and annealing cycle in a separate chamber, the sample was transferred through air to a Kel-F electrochemical cell [5]. The potential applied to the Au(110) sample is referenced to a Ag/AgCl(3*M* KCl) electrode. Measurements were carried out at room temperature with $\lambda = 1.53$ Å at NSLS beam lines X22B and X25. The scattering vector **Q** equals $(Ha^*, Kb^*, Lc^*)$ where $a^* = b^* = c^* = 2\pi/a$ and $a = 4.081$ Å (see Fig. 1). The longitudinal resolution, determined by the angular acceptance of the detector Soller slits, is $0.005a^*$ half width at half maximum (HWHM).

Figure 2(a) shows the scattered intensity along (0.1,0.1,*L*) [see Fig. 1(c)] at several potentials in 0.1*M* NaCl and $HClO_4$. The peaks at $L = 1$ and $L = 2$ arise from the diffuse rods of scattering (truncation rods) in the wings of the Bragg peaks. Other peaks—which do

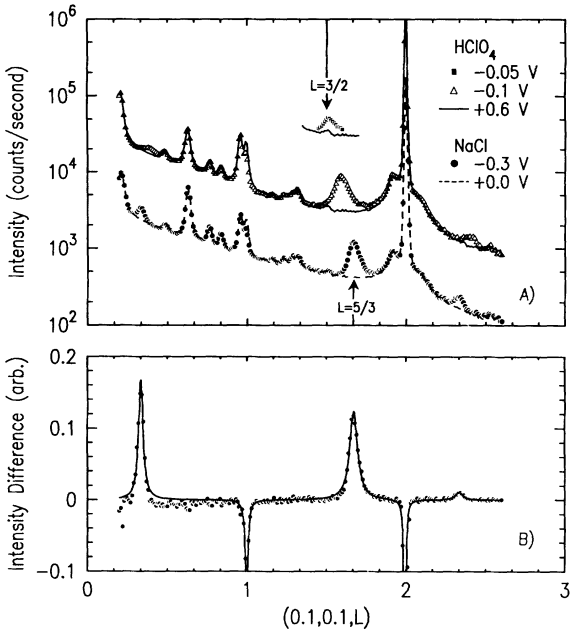


FIG. 2. (a) Diffraction intensity for the Au(110) electrode in 0.1$M$ $HClO_4$ and NaCl along (0.1,0.1,$L$) at several potentials. The peaks at $L=\frac{3}{2}$ and $\frac{5}{3}$ signify the (1×2) and (1×3) phases, respectively, for the $HClO_4$ and NaCl electrolytes. The curves for $HClO_4$ have been shifted upward for clarity. (b) The intensity difference (solid circles) between the −0.3 and 0.0 V curves in 0.1$M$ NaCl shown in (a). The solid lines are fits to Lorentzian profiles.

not depend on potential—are attributed to the scattering from the plastic windows and water. In $HClO_4$ a diffraction peak emerges at $L=\frac{3}{2}$ at 0.00 V [shown as squares in Fig. 2(a) at −0.05 V]. Diffraction at the half-order position supports the notion of a (1×2) reconstruction. With decreasing potential this peak moves to larger $L$ and by −0.3 V this incommensurate peak is centered midway between the (1×2) and (1×3) positions. An identical scattering profile is obtained after increasing the potential to −0.1 V [shown in Fig. 2(a) as triangles]. A diffraction peak at $L=\frac{5}{3}$ is never observed in $HClO_4$ and the peak at $L=\frac{3}{2}$ observed at −0.05 V in the negative sweep is never restored. Separate large domains of (1×2) in coexistence with domains of (1×3), as reported in Ref. [12] with STM, would give rise to diffraction peaks at both the third- and half-order positions, $L=\frac{5}{3}$ and $\frac{3}{2}$, respectively, and no peak midway between these two positions. The incommensurate diffraction profile is consistent with random sequencing models constructed from (1×2) and (1×3) rows [14,15].

By carrying out measurements in salt solutions the surface can be charged more negative than in acid solutions because the $H_2$ gas evolution starts at a more negative potential. We find that at negative potentials in the salt solution the Au(110) surface forms a (1×3) pattern and a (1×2) pattern is never observed. This is demonstrated by Fig. 2(a) where the diffraction data at −0.3 V exhibit peaks at $L=\frac{1}{3}$, $\frac{5}{3}$, and $\frac{7}{3}$ which are absent at 0.0 V. The background subtracted data are shown in Fig. 2(b). The noninteger diffraction peak positions are all within $0.005a^*$ of the third-order positions and the HWHM are all close to $0.03a^*$.

Analysis of the width of the diffraction profiles provides a direct measure of the size, $\zeta$, of the correlated domains. After potential cycling in the negative potential regime [5] the profile widths decreased by a factor of 2 from those shown in Fig. 2 and these data (not shown) are used in the following analysis. For an exponential correlation function in 1D, the scattering in reciprocal space is Lorentzian and the HWHM $\kappa$ is $1/\zeta$. Least-squares fits to a Lorentzian form, including the effect of the Gaussian spectrometer resolution, have been carried out and the best fit of the longitudinal profile, i.e., along $L$, in the vicinity of (0.1,0.1,$\frac{5}{3}$) and (0.1,0.1,$\frac{7}{3}$) gives $\zeta_l=50\pm5$ Å. This correlation length corresponds to about four periods of the (1×3) unit cell. In contrast, the transverse correlation, $\zeta_2=250\pm25$ Å. Whereas $\zeta_2$ is consistent with the longitudinal correlation length measured at the Au(111) and Au(001) surfaces [5], $\zeta_l$ at the Au(110) surface is a factor of 5 smaller. The short correlation length at the Au(110) surface is probably due to disorder between the missing rows [15].

The real space model for the (1×3) unit cell is deduced from quantitative measurements of the diffracted intensity along (0.1,0.1,$L$), from the specular reflectivity, and from the truncation rods at the third-order reflections. Whereas the surface rods at ($X$,$X$,$\frac{1}{3}$), ($X$,$X$,$\frac{5}{3}$), ($X$,$X$,$\frac{7}{3}$), ($X$,$X$,$\frac{11}{3}$), ($1+X$,$-1+X$,$\frac{2}{3}$), and ($1+X$, $-1+X$,$\frac{4}{3}$) are strongest at small $X$, unobservable near $X=0.9$, and peak again at $X=1.8$, the rods at ($X$,$X$,$\frac{2}{3}$), ($X$,$X$,$\frac{4}{3}$) exhibit the opposite trend. These observations, along with the sharp decrease of the specular reflectivity between the origin and the (2,2,0) Bragg peak are expected on the basis of the three-missing-row model [Fig. 1(b)] and exclude real space models in which only the top gold layer is partially occupied (one or two missing rows).

The in-plane distortions of the (1×3) reconstruction can be related to the integrated intensity obtained in the grazing incidence geometry [16]. A pairing distortion of the second layer, that is, an outward lateral displacement of the atoms, shown by the arrows in Fig. 1(b), is the in-plane distortion closest to the surface. Within the context of this model, the lateral separation between the atoms in the second layer expands to accommodate the inward relaxation of the atoms in the top layer. If the atoms are displaced laterally by a distance $\delta a$ from their undistorted sites, then the in-plane structure factor, $S(H=0,K=0,L)$, equals $|1+2\cos(\pi L[1+2\delta])|^2$ at $L=\frac{1}{3}$, $\frac{2}{3}$, $\frac{4}{3}$, $\frac{5}{3}$, $\frac{7}{3}$, $\frac{8}{3}$, etc. In the absence of the pairing distortion, i.e., $\delta=0$, $S(0,0,L)=4$ at $L=\frac{1}{3}$, $\frac{5}{3}$, $\frac{7}{3}$, and $\frac{11}{3}$, and $S=0$ for $L=\frac{2}{3}$, $\frac{4}{3}$, and $\frac{8}{3}$. The fact that the corrected intensi-

ty ratio between $(0.1,0.1,\frac{5}{3})$ and $(0.1,0.1,\frac{7}{3})$ is 0.15 and not unity strongly suggests the presence of lateral displacements. By including the pairing distortion, the best fit is obtained with the second-layer atoms displaced laterally by about 0.14 Å ($\delta=0.035$) from their undistorted positions.

In order to ascertain the surface normal structure of the (1×3) phase, the absolute specular reflectivity was obtained at −0.3 V using techniques described in Ref. [5]. Between the origin and the (2,2,0) Bragg peak, the reflectivity is much lower than the reflectivity from an ideal (1×1) surface (Fig. 3). This is because the electron density profile decays more gradually in the (1×3) missing-row model than for the ideally terminated (1×1) phase. By analyzing the reflectivity in terms of simple sums over atomic layers, we have obtained the layer densities, surface normal relaxation parameters, and rms displacement amplitudes. We have fitted the specular reflectivity—excluding the data with $H$ less than 0.5—to the relaxed (1×3) missing-row model. The best fit (solid line in Fig. 3) provides an excellent description of the data. The fitted rms displacement amplitudes for the top three layers are greater than the bulk Debye-Waller value of 0.09 Å. We find that the top and second layers contract by 16% and 7%, respectively, relative to the undistorted bulk layers, and that the third layer buckles [9] by 3.2%. This is close to the 18% contraction measured for the (1×2) structure in vacuum [7] and to first-principles calculations [17]. These same calculations have been extended to the (1×3) reconstruction and the contraction is close to 20% [17]. The adsorption of Cs in vacuum induces a (1×3) reconstruction [9]; however, the 31% contraction of the top layer (relative to the bulk) is significantly greater than our measured value of 16% and the value obtained from calculations [17]. In all of these studies the top layer is contracted and this produces a smoother surface than the unrelaxed missing-row structures.

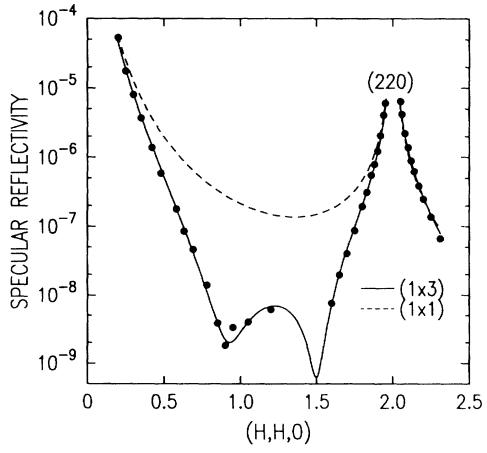


FIG. 3. Specular x-ray reflectivity from the Au(110) electrode in 0.1$M$ NaCl in the (1×3) phase. The solid line is the best fit to the reflectivity using a (1×3) three-missing-row structure. The dashed line is for an ideal (1×1) surface.

Figure 4 shows the normalized scattering intensity at three wave vectors versus the applied potential. At $(0.1,0.1,\frac{5}{3})$ [Fig. 4(b)] the scattered intensity increases from zero at high potentials where the surface has (1×1) symmetry, as the reconstruction starts to form (at approximately −0.1 V). This increase is preceded by a decrease in the reflectivities in the wings of the (1,1,1) and (2,2,0) Bragg peaks and this effect is demonstrated by the potential scans at (0.7,0.7,1) and (1.7,1.7,0), respectively, in Figs. 4(c) and 4(d). This intensity decrease in going from the (1×1) to (1×3) phase is associated with a gold density profile at the surface which decays gradually along the surface normal direction in the (1×3) phase. Hysteresis in the scattered intensity is observed at all three positions. However, this effect is reduced at the specular position (1.7,1.7,0) since the reflected intensity is not very sensitive to the in-plane atomic positions. On account of this hysteresis, the transition between the (1×1) and (1×3) phases appears to be first order.

In order to correlate the x-ray scattering measurements with electrochemical data, differential capacitance measurements have been carried out in a different cell at a scan rate of 8 mV/sec. As shown in Fig. 4(a), there is frequency dispersion over the potential range from −0.5

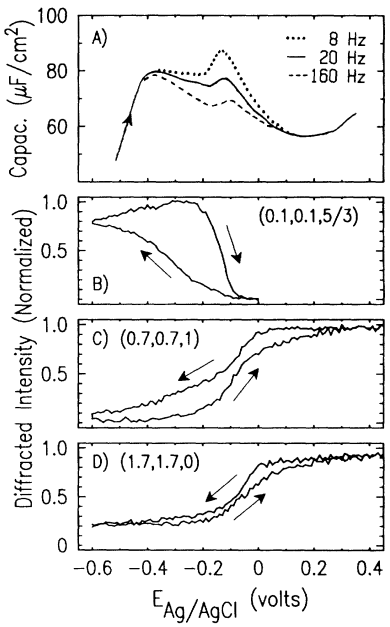


FIG. 4. (a) Differential capacitance from the Au(110) surface in 0.1$M$ NaCl at several frequencies. (b)–(d) Potential dependence of the scattered intensity from the Au(110) electrode in 0.1$M$ NaCl at 1 mV/sec sweep rate. Normalized intensities are calculated by subtracting the diffuse background and normalizing to unity at the highest value.

to 0.0 V and at the lower frequencies there is a well-defined capacitance peak at $-0.12$ V. This potential corresponds exactly to the potential where the x-ray intensity at $(0.1,0.1,\frac{5}{3})$ falls to half of its value in the reconstructed potential range. Furthermore, the width of the capacitance peak is in agreement with the potential range over which the $(1\times3)$ phase vanishes.

In addition to the NaCl measurement, we have carried out studies in NaF, NaBr, LiCl, and CsCl salt solutions. For all of the salt electrolytes, in the negative potential regime, a scattering peak at $L=1.67\pm0.02$, characteristic of the $(1\times3)$ structure, is observed. Therefore, the cation and anion species do not significantly affect the structure of the reconstructed Au(110) surface for these salt solutions. However, the phase transition potential depends on the anion species. The transition potential, defined as the potential where the intensity at $(0.1,0.1,\frac{5}{3})$ falls to half in a positive potential sweep, is 0.09 V in NaF, $-0.13$ V in NaCl, and $-0.33$ V in NaBr. In LiCl and CsCl the transition occurs at $-0.14$ and $-0.16$ V, respectively, and the close agreement with the NaCl value suggests that the cation remains nearly fully hydrated at the interface.

In comparison, Ag(110), which is unreconstructed in vacuum, forms a $(1\times2)$ phase after the adsorption of K [18]. This transition to a $(1\times2)$ structure is in agreement with free energy models for silver which incorporate the effect of surface charge [19]. In the context of these calculations, the relative stability of the $(1\times2)$ and $(1\times3)$ phases has not been considered. Further theoretical calculation, which include the effect of surface charge on the stability of the $(1\times1)$, $(1\times2)$, and $(1\times3)$ phases of gold might provide a theoretical basis for our thesis that excess surface charge favors the $(1\times3)$ phase relative to the $(1\times2)$ phase.

In summary, we have measured the *in situ* phase behavior of the Au(110) surface in salt and $HClO_4$ solutions versus the applied potential. When the surface is negatively charged in salt solutions a relaxed $(1\times3)$ gold structure is formed. This structure does not depend on the anion or cation. In contrast, in $HClO_4$ a poorly correlated structure is formed which is intermediate between the $(1\times2)$ and $(1\times3)$ structures. The differences between the salt and acid results cannot be attributed to the specific adsorption of ions since these cations remain solvated at the interface in either case. The $(1\times3)$ reconstruction in salt solutions is consistent with the structure observed in UHV after the adsorption of small concentrations of alkali metals and with our supposition that a sufficiently negative surface charge induces a $(1\times3)$ rather than a $(1\times2)$ reconstruction.

We would like to thank Gary Ownby, David Zehner, and Doon Gibbs. This work is supported by the Division of Materials Research, U.S. Department of Energy, under Contract No. DE-AC02-76CH00016. One of us (G.H.) would like to acknowledge the Research Council of Norway.

[1] X. Gao, A. Hamelin, and M. J. Weaver, Phys. Rev. Lett. **67**, 618 (1991); J. Chem. Phys. **95**, 6993 (1991).
[2] S. L. Yau *et al.*, J. Am. Chem. Soc. **113**, 6049 (1991); O. M. Magnussen *et al.*, Phys. Rev. Lett. **64**, 2929 (1990).
[3] S. Manne *et al.*, Science **25**, 183 (1991).
[4] M. F. Toney *et al.*, Langmuir **7**, 796 (1991), and references therein.
[5] B. M. Ocko, J. Wang, A. Davenport, and H. Isaacs, Phys. Rev. Lett. **65**, 1466 (1990); J. Wang, A. J. Davenport, H. S. Isaacs, and B. M. Ocko, Science **255**, 1416 (1992).
[6] W. Moritz and D. Wolf, Surf. Sci. **163**, L655 (1985); S. H. Overbury *et al.*, Surf. Sci. **109**, 239 (1981); G. Binning *et al.*, Surf. Sci. **247**, 327 (1991).
[7] E. Vleig, I. K. Robinson, and K. Kern, Surf. Sci. **233**, 248 (1990).
[8] D. K. Flynn-Sanders *et al.*, Surf. Sci. **253**, 2701 (1991).
[9] P. Häberle, P. Fenter, and T. Gustafson, Phys. Rev. B **39**, 5810 (1989).
[10] A. Hamelin, J. Electroanal. Chem. **142**, 299 (1982).
[11] M. S. Zei, G. Lempful, and D. M. Kolb, Surf. Sci. **221**, 23 (1989); R. Michaelis and D. M. Kolb, Surf. Sci. **234**, L281 (1990).
[12] X. Gao, A. Hamelin, and M. J. Weaver, Phys. Rev. B **44**, 10983 (1991).
[13] D. M. Zehner (private communication).
[14] S. Hendricks and E. Teller, J. Chem. Phys. **10**, 147 (1942); P. J. Eng and I. K. Robinson (private communication).
[15] J. Villain and I. Vilfan, Surf. Sci. **199**, 165 (1988).
[16] The integrated intensities in a $\theta$ scan have been corrected to include the effects of the Lorentz factor ($\sin[2\theta]$), atomic form factor, Debye-Waller factor, the synchrotron polarization factor, and the profile width along $L$.
[17] K. M. Ho and K. P. Bohnen, Europhys. Lett. **4**, 345 (1987); K. P. Bohnen (private communication).
[18] B. E. Hayden *et al.*, Phys. Rev. Lett. **59**, 2307 (1987); C. J. Barnes *et al.*, Surf. Sci. **219**, 143 (1989).
[19] C. L. Fu and K. M. Ho, Phys. Rev. Lett. **63**, 1617 (1989).

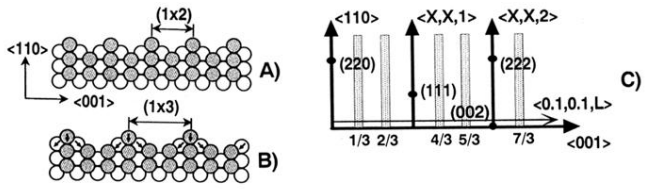


FIG. 1. Cross-sectional view of the (a) $(1\times2)$ and (b) $(1\times3)$ missing-row models of the reconstructed Au(110) surface. The surface scattering geometry is shown in (c).